Available online at www.sciencedirect.com
ScienceDirect
Remote Sensing of Environment 107 (2007) 334–347
Remote Sensing of Environment
www.elsevier.com/locate/rse

Analysis of the MISR LAI/FPAR product for spatial and temporal coverage, accuracy and consistency

Jiannan Hu [a], Yin Su [a], Bin Tan [a], Dong Huang [a], Wenze Yang [a], Mitchell Schull [a], Michael A. Bull [b], John V. Martonchik [b], David J. Diner [b], Yuri Knyazikhin [a,*], Ranga B. Myneni [a]

[a] Department of Geography, Boston University, 675 Commonwealth Avenue, Boston, MA 02215, USA
[b] Jet Propulsion Laboratory, Pasadena, CA 91109, USA

Received 1 March 2006; received in revised form 8 June 2006; accepted 16 June 2006

Abstract

The Multi-angle Imaging SpectroRadiometer (MISR) instrument provides global imagery at nine discrete viewing angles and four visible/near-infrared spectral bands. MISR standard products include green leaf area index (LAI) of vegetation and fraction of photosynthetically active radiation absorbed by vegetation (FPAR). This paper describes the research basis for transitioning the MISR LAI/FPAR products from provisional to validation status. The efforts included not only comparisons to field data but also analyses of relationships, consistency and complementarity between various MISR products derived by independent algorithms. For example, we show how the energy absorbed by the ground below vegetation can be estimated from two independent MISR products, FPAR and BHRPAR (bi-hemispheric reflectance at PAR wavelengths). Further, we show that this information can be used to derive at least three measures of canopy structure — Beer's law extinction coefficient, mean leaf inclination and the gap fraction or vegetation ground cover. The spatial and temporal coverage of the LAI/FPAR product is mainly limited by cloud contamination. However, when a successful aerosol retrieval is performed, typically 95% of pixels have surface reflectance retrievals suitable as input to the LAI/FPAR algorithm. The algorithm provides LAI/FPAR retrievals in 50–80% of these pixels with suitable input. The early versions of the algorithm overestimated LAI values in grasses and broadleaf crops. The MISR LAI product from the recalibrated algorithm (version 3.3) is assessed by comparison with field data collected in a 3×3 km agricultural area (grasses and cereal crops) near Avignon, France. LAI retrievals in other biomes are compared to MODIS LAI product of known accuracy. The MISR LAI product shows structural and phenological variability in agreement with data. Our results suggest that the product is accurate to within 0.66 LAI in herbaceous vegetation and savannas and is an overestimate by about 1 LAI in broadleaf forests. LAI retrievals over needle leaf forests remain at provisional quality level.

Keywords: MISR; Leaf area index; Fraction of photosynthetically active radiation absorbed by vegetation; Satellite product

1. Introduction

The multi-angle imaging spectroradiometer (MISR) instrument is designed to provide global imagery at nine discrete viewing angles and four visible/near-infrared spectral bands. The MISR team is responsible for development and validation of algorithms and for producing a series of products which include vegetation green Leaf Area Index (LAI) and Fraction of Photosynthetically Active Radiation (400–700 nm) absorbed by vegetation (FPAR). These products are required to describe the exchange of fluxes of energy, mass (e.g., water and CO_2) and momentum between the surface and atmosphere (Sellers et al., 1997).

MISR LAI/FPAR research has three major components — algorithm development, product analysis and validation. Algorithm development includes the development of the at-launch algorithm (Knyazikhin et al., 1998a,b), prototyping of the algorithm prior to the launch of Terra platform (Zhang et al., 2000), and algorithm refinement (Hu et al., 2003). Product analysis includes assessment of the overall algorithm performance at global scale and assessment of the accuracy and quality of the product at regional scales with emphasis on understanding how input data uncertainties impact retrieval quality (Wang et al., 2001; Hu et al., 2003).

* Corresponding author. Tel.: +1 617 353 8843; fax: +1 617 353 8399.
E-mail address: jknjazi@bu.edu (Y. Knyazikhin).

0034-4257/$ - see front matter © 2006 Elsevier Inc. All rights reserved.
doi:10.1016/j.rse.2006.06.020

This paper describes the research basis for transitioning the MISR LAI/FPAR product from provisional to "stage 1 validation" status defined as "Product accuracy has been estimated using a small number of independent measurements obtained from selected locations and time periods and ground-truth/field program effort" (WWW1). An infrastructure presently exists that accumulates resources required for validation of satellite products (Morisette et al., 2006). At most of the sites included in this structure, there is a long-term measurement program to support in situ measurements that can be used to assess the quality of satellite products. Data available through the existing infrastructure are used in this research to establish the stage-1 validation status of MISR LAI/FPAR products.

The assessment of the quality of satellite-derived parameters should include not only validation but also a comprehensive analysis of relationships, consistency and complementarity between various products derived from independent algorithms. Such an analysis is valuable to establishing product accuracies and demonstrating their utility for monitoring and modeling studies. This aspect of product quality assessment is also discussed in this paper.

The paper is organized as follows. Section 2 provides background information on the MISR Level 2 surface parameters product. The information content of MISR surface parameters, their consistency and complementarity, as well as their utility for monitoring and modeling studies are analyzed in Section 3. The spatial and temporal coverage of the MISR Level 2 surface product over different validation sites is examined in Section 4. The validation results from five vegetation sites are presented in Section 5. Finally, the concluding remarks are summarized in Section 6.

2. Description of the MISR surface parameters product

The MISR instrument on the Earth Observing System (EOS) Terra platform orbits the Earth about 15 times each day. There are 233 distinct orbits, called paths, which are repeated every 16 days, and since the paths overlap, near global coverage is obtained in 9 days. The MISR instrument views symmetrically about the nadir in forward and afterward directions along the spacecraft flight track. Image data are acquired with nominal view zenith angles relative to the surface reference ellipsoid of 0.0°, 26.1°, 45.6°, 60.0° and 70.5° in four spectral bands (446, 558, 672, and 866 nm). The MISR data are distributed from the NASA Langley Atmospheric Sciences Data Center (WWW2). The MISR products are archived for each path and orbit. The orbit number corresponds to data acquired over a path for a particular date. Each path is about 360 km wide from east to west which, in turn, is divided into 180 blocks measuring 563.2 km (cross-track) × 140.8 km (along-track), that is, 512 × 128 pixels. For a given path, a numbered block always contains the same geographic locations.

The MISR Level 2 Land Surface Product is at a spatial resolution of 1.1 km and includes spectral hemispherical-directional reflectance factors (HDRF) at the nine MISR view angles and the associated bihemispherical reflectance (BHR). The HDRF is the ratio of the directionally reflected radiance from the surface to the reflected radiance from an ideal lambertian target under identical illumination conditions as the surface. The BHR is the HDRF integrated over all reflection angles in the upward hemisphere, i.e., it is the surface spectral albedo under ambient atmospheric illumination. Related MISR surface parameters, also being generated and archived within the Land Surface Product, are the spectral bidirectional reflectance factor (BRF) at the nine MISR view angles and the directional-hemispherical reflectance (DHR). The BRF and the DHR characterize the surface in the same way as the HDRF and BHR, respectively, but are defined for the condition of direct illumination only. In addition to these spectral products, the BHR and DHR, integrated over the wavelength region of photosynthetically active radiation (PAR) (400–700 μm), BHRPAR, are also computed. The details of the retrieval methodologies used to derive these products have been described by Martonchik et al. (1998b).

The MISR Level 2 Land Surface Product also includes vegetation green leaf area index (LAI) and the fractional amount of vegetation absorbed photosynthetically active radiation (FPAR). The LAI is defined as the one-sided green leaf area per unit ground area in broadleaf canopies and as the projected needle leaf area per unit ground area in coniferous canopies. The FPAR is defined for ambient sky conditions, i.e., it accounts for both diffuse and direct illumination. In the MISR approach to LAI/FPAR retrievals, global vegetation is stratified into six canopy architectural types or biomes (Myneni et al., 1997). The six biomes are grasses and cereal crops (biome 1), shrubs (biome 2), broadleaf crops (biome 3), savannas (biome 4), broadleaf forests (biome 5) and needle leaf forests (biome 6). For each biome, the LAI/FPAR algorithm first identifies all LAI values and soil and/or understory reflectances for which modeled and observed BHR and BRF differ by an amount equivalent to or less than the combined uncertainty in model and observations. FPAR is calculated for each such LAI and soil or understory reflectance. Second, from this set, conditional mean LAI and FPAR and their dispersions are calculated. The conditional mean LAI and FPAR are defined as the LAI and FPAR averaged over all soil or understory models for a given biome type. Finally, the most probable LAI, FPAR and biome type are chosen, using the results from the biome which has the least coefficient of variation (dispersion divided by mean). The conditional LAI values, their spread as well as the most probable values of LAI and FPAR are archived in the MISR Surface Parameters Product for each 1.1 km MISR pixel within which the BHR/BRF retrieval was performed. The details of the retrieval methodologies used to derive these products can be found in (Hu et al., 2003; Knyazikhin et al., 1998a,b). Here the emphasis will be on the conditional LAI parameter. The most probable values of LAI and FPAR are analyzed in Hu et al., 2003.

3. Examples of MISR retrieval quality, uniqueness and consistency

Product assessment should include, in addition to validation efforts, a comprehensive analysis of the relationships, consistency and complementarity between various parameters derived

from independent algorithms. Such an analysis highlights the utility of these parameters for studies on monitoring and modeling as well as for exploring the potential for enhanced information retrieval through innovative manipulation of multiple parameters. Here, a select number of retrieval cases are presented to showcase the information content of surface directional reflectances, consistency and complementarity between the various parameters of the MISR surface product suite.

3.1. Angular signatures in spectral space

A vegetated surface scatters shortwave radiation into an angular reflectance pattern, whose magnitude and shape are governed by the composition, density, optical properties and geometric structure of the vegetation canopy and its underlying surface. Zhang et al. (2002a,b) have shown that the angular signatures at different spectral bands are not independent and their correlation conveys information about canopy structure. The correlation, e.g., can be seen if one depicts variation in the BRF at red and near-infrared (NIR) wavelengths with the view angle (Fig. 1). Points corresponding to different view angles form a curve — an angular signature in spectral space (Zhang et al., 2002a). The signature can be characterized by three metrics: (i) its location in the spectral space, which is mainly determined by the biome type; the DHR at red and NIR wavelengths is used to specify the location; (ii) inclination (slope and intercept) of the signature, which is determined by leaf and soil optical properties, and the structure of the canopy; and (iii) the length of the signature, which describes spectral variation in the shape of the BRF. Here we follow a methodology to interpret multi-angle data proposed by Zhang et al. (2002a,b).

The mean signatures of 2 by 2 degree areas representative of five biomes and corresponding to the greenest seasons are shown in Fig. 2. The selected areas are centered on the following EOS Core Validation Cites (WWW1): Konza Prairie Biological Station, Manhattan, Kansas, USA (39.0823°N, 96.56025°W); Bondville, a cropland site in Illinois, USA (40.007°N, 88.292°W); Harvard Forest, a temperate mixed forest site in Massachusetts, USA (42.529°N, 72.173°W); Walnut Gulch (San Pedro), a shrubland/grassland mixture site in Arizona, USA (31.74N, 109.94W); and BOREAS Northern Study Area (NSA), a needleleaf forest site in Manitoba, Canada (55.87N, 98.48W).

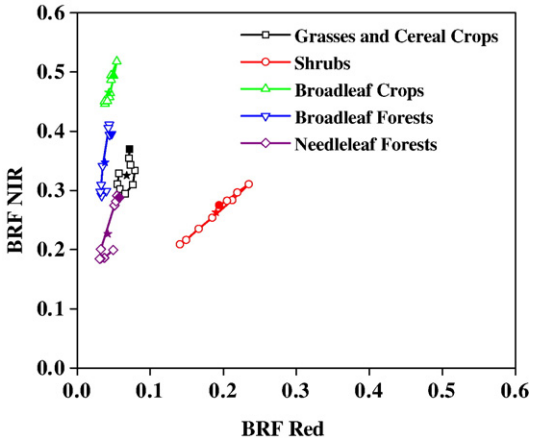

Fig. 2. Angular signatures on the RED vs. NIR plane for five land covers. The solar zenith angle and the azimuth angle of the BRFs measured from the principal plane are 19°±1° and 51°±10° for Grasses and Cereal Crops (June, 2000); 25°±3° and 50°±10° for Shrubs (April, 2000), 24°±1° and 60°±15° for Broadleaf Crops (July, 2000); 33°±2° and 40°±8° for Broadleaf Forests (August, 2000); 42°±3° and 60°±10° for Needleleaf Forests (August, 2000). The locations, or DHRs in red and NIR spectral bands, are depicted as stars. The solid symbol on each curve indicates the 70.5° afterward camera. (For interpretation of the references to colour in this figure legend, the reader is referred to the web version of this article.)

The location of reflectance data in the spectral space is the basic source of information about the vegetation canopy conveyed by single-angle multi-spectral satellite data. In our example, the locations of broadleaf crops, broadleaf and needleleaf forests, shrubs, and to some extent grasses and cereal crops are distinct in the red-NIR space. Needle forests appear darkest in these plots. Multiple photon-needle interactions within shoots are primarily responsible for this phenomenon (Rautiainen & Stenberg, 2005; Smolander & Stenberg, 2003, 2005).

The length of the signature is another type of information provided by multi-angle data about canopy structure. It measures the degree of anisotropy in the reflected radiation field which is dependent on the heterogeneity of the medium. For the

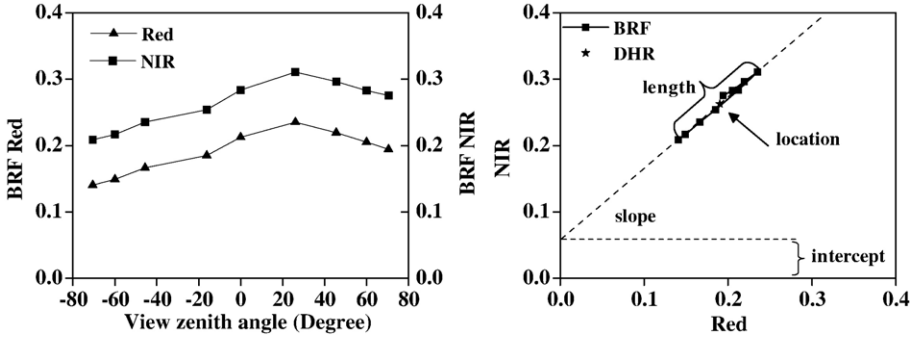

Fig. 1. Left panel: Angular variation of BRF in red and NIR spectral bands for shrubs. The solar zenith angle and the azimuth angle measured from the principal plane are 25°±3° and 50°±10°, respectively. Right panel: Values of the BRF at red and NIR wavelengths as a function of the view zenith angle form a curve on the RED vs. NIR plane, or, angular signature in spectral space (Zhang et al., 2002a). The signature is characterized by three metrics: (i) its location in the spectral space which is determined by the directional hemispherical reflectance (DHR), (ii) inclination (slope and intercept) of the signature, and (iii) the length of the signature, which describes spectral variation in the shape of the BRDF.

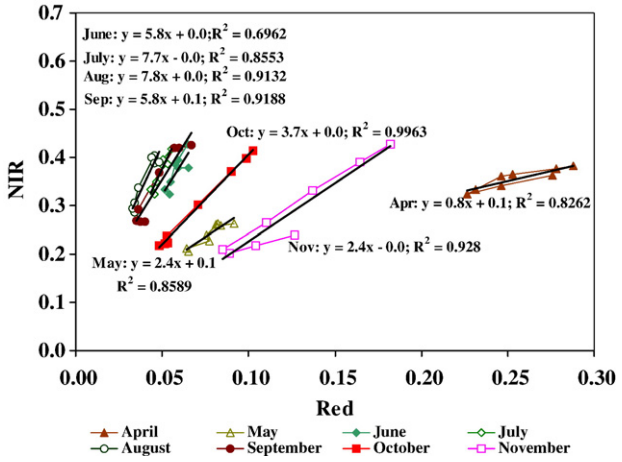

Fig. 3. Temporal variation in the mean signature of a broadleaf forest located in the 2 by 2 degree area centered on the Harvard Forest EOS Core Validation Site (42.529°N, 72.173°W). The MISR data acquired from March to November, 2000 were used to derive these signatures.

case of a homogeneous medium, defined as an isotropic reflector, the length is zero because the angular signature in spectral space is a point. One can see that shrubs have the highest length values relative to other biomes, thus indicating a high degree of both lateral and vertical heterogeneity. The forest biomes exhibit larger length magnitudes compared to grasses and crops. This indicates a higher degree of vertical heterogeneity in the case of forests (Zhang et al., 2002a).

In terms of inclination of the signature, forest biomes tend to have steeper slopes and smaller intercept values. Shrubs, on the other hand, show the lowest slope and a large intercept. In the case of dense vegetation canopies, the ratio between BRFs at near infrared and red spectral bands, or the simple ratio (SR), is nearly independent of view directions, indicating a low impact of canopy background on the BRF (Kaufmann et al., 2000; Zhang et al., 2002a). The fact that sparse vegetations tend to have a non-zero intercept indicates a sensitivity of the simple ratio to view and sun angle variations. This is because the surface reflectance results from contributions of radiation reflected by vegetation (e.g., shrub) and ground which vary nonlinearly with view angle.

The temporal movement of data in the spectral space characterizes changes in canopy properties (Shabanov et al., 2002). Fig. 3 shows the seasonal change in the mean signature of a broadleaf forest located in a 2 by 2 degree area centered on the Harvard Forest site. In April, the trees are leafless and hence LAI is equal to zero. The corresponding signature is mainly determined by the reflectance and anisotropy of a bare background. A non-zero intercept and a low value of the slope make the simple ratio sensitive to view angle. As LAI increases from May to July, the signature moves in the spectral space away from its location in April. This movement is accompanied by a sharp decrease in the red and an increase in the NIR reflectance. The slope jumps from 2.4 in May to its maximum value of about 7.7 in July and August. In these summer months, the simple ratio is insensitive to the view angle. The length reaches its minimum value, indicating the lowest degree of the horizontal heterogeneity. The location corresponding to the greenest seasons depends mainly on the leaf optical properties (Zhang et al., 2002b). The September signature still has a steep slope. It occupies approximately the same space on the RED vs. NIR plane as in July and August. These two features suggest a low impact of background on canopy reflectance (Zhang et al., 2002b). However, changes in the leaf optics result in an increased value of the signature length. The decrease in the slope and increase in the length from October to November indicate a stronger impact of the background on reflected radiation and, consequently, a lower LAI value.

3.2. LAI and FPAR retrievals over sparse vegetation

Shrubs have low vegetation cover over a bright background and exhibit lateral spatial heterogeneity. According to the Collection 4 MODIS Land Cover Product (WWW3), this biome constitutes about 25% of global vegetation. Fig. 4 shows the annual course of LAI and FPAR derived from MODIS and MISR data for a 2 by 2 degree area centered on the Walnut Gulch (San Pedro) site in Arizona (WWW1). The MISR product exhibits seasonality while the MODIS product is almost

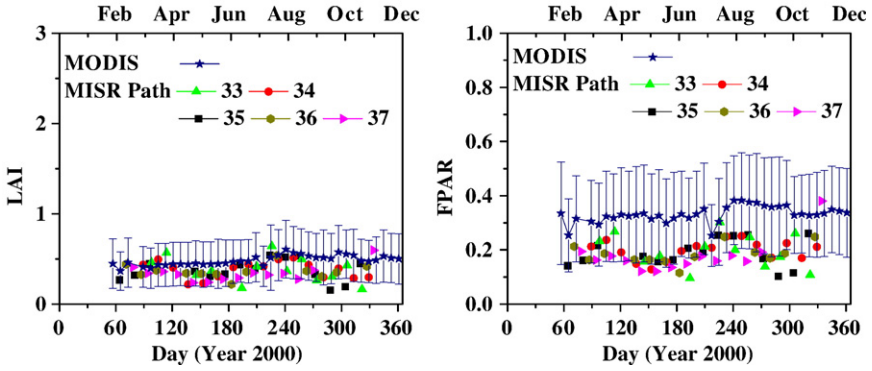

Fig. 4. Annual course of leaf area index (left panel) and fraction vegetation absorbed PAR (right panel), for year 2000, from MODIS and MISR data for the Walnut Gulch (San Pedro) site in Arizona, (31.74N, 109.94W). Symbols in the MISR LAI and FPAR profiles correspond to mean values over different paths overlapped with 2° by 2° areas centered on the flux tower site. The most probable LAI and FPAR are used.

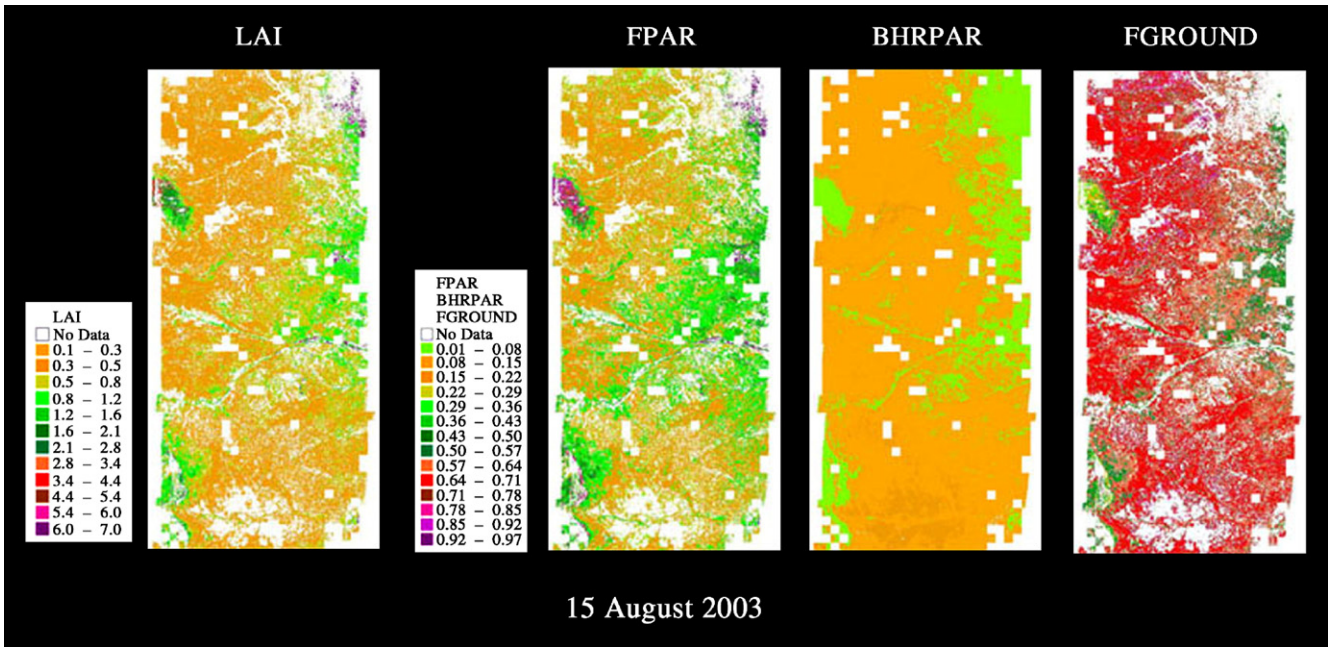

Fig. 5. Partitioning of the top-of-canopy PAR into its canopy and ground absorbed portions. The MISR Land Surface Product includes leaf area index (LAI), fraction of photosynthetically active radiation absorbed by vegetation (FPAR) and bihemispherical reflectance integrated over the photosynthetically active spectral region (BHRPAR). From these products, the fraction of PAR absorbed by the ground can be estimated as 1 − BHRPAR − FPAR. MISR Level 2 Land Surface Data over North America from 15 August 2003 (path 32, orbit 19461), blocks 54–60 are shown here. Latitude and longitude of the image upper left (lower right) corner are 46.54° (37.13°) and −104.28° (−100.09°), respectively. The most probable LAI and FPAR are used.

flat. This seasonality is consistent with the response of the vegetation to precipitation in this region, which is bi-modally distributed with about 50 to 60% of the annual total of about 76 cm falling in the summer monsoon season, and 21% to 35% occurring in the winter months.

The MODIS and MISR algorithms both perform retrievals by comparing observed and modeled radiances for a suite of canopy structure and soil patterns that covers a range of expected natural conditions (Knyazikhin et al., 1998a,b). The set of all canopy and soil patterns for which the magnitude of the residuals in the comparison does not exceed uncertainties in observed radiances is treated as acceptable solutions. FPAR is calculated for each such LAI and soil or understory reflectance. The mean LAI and FPAR over all acceptable LAI values are taken as the retrieved LAI and FPAR values. The information conveyed about canopy structure is small in the case of a single-angle instrument whose footprint does not spatially resolve individual scene elements. Therefore, a wide range of natural variation in LAI and soil or understory reflectance can result in the same value of the remotely sensed signal. This results in a higher uncertainty in retrieved values of LAI and FPAR. Since the interaction of photons with canopy structure determines the directional reflectance distribution, the use of multi-angle information results in fewer solutions that are consistent with the observations. The retrieval uncertainty in LAI is therefore low. A comparison of MODIS and MISR LAI retrievals with field data supports this inference (Section 5.2). This example demonstrates the advantage of multi-angle data for retrievals in arid land — marginal ecosystems that are dynamic and being subject to anthropogenic pressures.

3.3. Partitioning of solar radiation

LAI and FPAR are parameters that are descriptive of vegetation canopy structure and its energy absorption capacity, and are key state variables in most ecosystem productivity models and in global models of climate, hydrology, and ecology (Sellers et al., 1997). For example, Buermann et al. (2001) reported that the use of satellite LAI reduces the model biases in near-surface air temperature in comparison to observations. The model was NCAR Community Climate Model 3 (Kiehl et al., 1996, 1998). The analysis showed how the use of satellite LAI fields allowed a more realistic partitioning of incoming solar radiation between the canopy and the ground below the canopy, thus resulting in improved model predictions of near-surface climate. This also highlighted the need for independent estimates of vegetation and ground absorption of solar radiation to describe the energy balance correctly.

The MISR surface product includes bihemispherical reflectance integrated over the photosynthetically active spectral region (BHRPAR), the broadband visible albedo. From energy conservation, the fraction of PAR absorbed by the ground beneath the canopy is given by the formula FGROUND = 1 − BHRPAR − FPAR. Fig. 5 shows the MISR standard surface product suite that includes LAI, FPAR and BHRPAR and the new parameter, FGROUND, derived from the standard products. In this example, BHRPAR is nearly homogeneous spatially. Thus the amount of PAR absorbed by the surface is also homogeneous. However, its partitioning between the vegetation and ground can be dramatically different. For example, from the LAI panel we note considerable spatial variation in

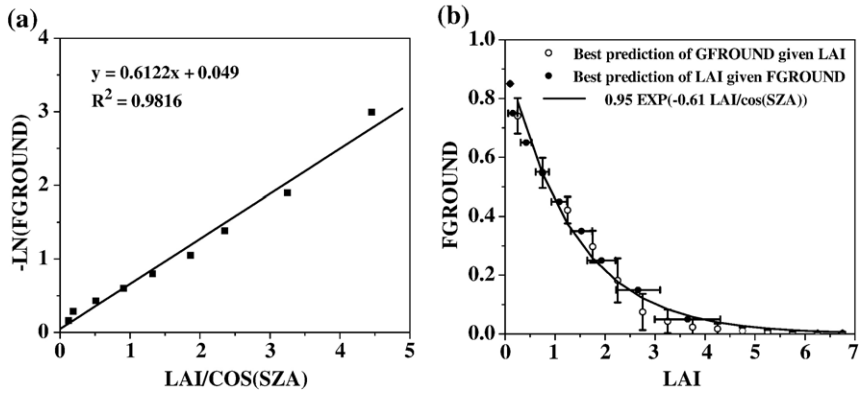

Fig. 6. (a): Using MISR Level 2 Land Surface Data over Africa from 23 April 2002 (path 176, orbit 12480, blocks 76–118), the negative logarithm of FGROUND is plotted against mean LAI normalized to the cosine of the solar zenith angle. The linear relation shows that mean LAI and FGROUND follows Beer's law. (b) Distribution of points $[F_1(f), f]$ and $[l, F_2(l)]$ on the FGROUND vs. LAI plane. Here LAI$=F_1(f)$ is the best possible prediction of LAI given a realized value, f, of FGROUND; FROUND$=F_2(l)$ is the best possible prediction of FGROUND given a value, l, of LAI. The most probable LAI and FPAR are used.

LAI. Not surprisingly, FPAR is also spatially variable and, consequently, the energy absorbed by the ground. This example suggests that the BHRPAR, or generally the albedo, alone does not convey adequate information in many cases.

3.4. Obtaining new information on canopy structure from MISR products

Given LAI and FGROUND fields, two types of regression curves can be derived. The first one, the best possible prediction of LAI given a realized value of FGROUND, LAI$=F_1(f)$, is the expectation of observed LAI under the condition that the FGROUND takes a given value f (Bronshtein & Semendyayev 1985, pp. 615–616). Similarly, the best possible prediction of FGROUND given a LAI value L, i.e., FGROUND$=F_2(L)$, can be obtained by averaging FGROUND values over pixels for which LAIs fall in a sufficiently narrow interval around a given value L. If there is a one-to-one relationship between LAI and FGROUND the functions F_1 and F_2 are reciprocally related; that is, $F_2(L)=F_1^{-1}(L)$. Fig. 6a shows the relationship between the negative logarithms of FGROUND and mean LAI normalized by the cosine of the solar zenith angle. The predicted LAI and FGROUND are related as FGROUND$=0.95\cdot\exp[-0.61\cdot\mathrm{LAI}/\cos(\theta_0)]$ where $\theta_0=35^0$ is the solar zenith angle. Panel (b) shows the distribution of points $[F_1(f), f]$ and $[L, F_2(L)]$ on the FGROUND vs. LAI plane. Their joint distribution can be well approximated by the exponential function shown in Fig. 6a. This indicates a strong relationship between LAI and FGROUND at the resolution of MISR products. These results can be interpreted as follows (Diner et al., 2005).

The fraction of PAR absorbed by the ground is the downward PAR flux density, F, times the soil absorptance, $1-\alpha$, where α is the reflectance of the canopy background. The downward flux, in turn, can be expressed via the downward flux density, F_{BS}, calculated for a vegetation canopy bounded by a non-reflecting surface as $F=F_{\mathrm{BS}}/(1-\alpha r^*)$ where r^* is the probability that photon entering through the lower canopy boundary will be reflected back by the vegetated layer (Knyazikhin & Marshak, 2000; Wang et al., 2003). Since green leaves usually absorb 85%–90% of intercepted radiation in the photosynthetically active region of the solar spectrum, F_{BS} can be approximated by the fraction of direct incident PAR that the vegetation canopy transmits. This fraction follows Beer's law, given by $\exp[-G(\theta_0)\cdot\mathrm{LAI}/\cos(\theta_0)]$, where θ_0 is the solar zenith angle, and $G(\theta_0)$ is a geometric factor defined as the projection of unit leaf area onto a plane perpendicular to the illumination direction (Ross, 1981). Thus,

$$\mathrm{FGROUND}=\frac{1-\alpha}{1-\alpha r^*}\exp[-G(\theta_0)\mathrm{LAI}/\cos(\theta_0)]. \quad (1)$$

The relationship between LAI and FGROUND derived from MISR data (Fig. 6) follows this equation with $(1-\alpha)/(1-\alpha r^*)=0.95$ and G(35°)$=0.61$. The following new information can be obtained from this equation.

According to de Wit's (1965) classification (see also Ross, 1981, pp. 92 and 116–117), the value $G(\theta_0)=0.61$ at SZA$=35°$ corresponds to a canopy with leaves between a planophile (mostly horizontal leaves) and plagophile (mostly leaves at 45°) type of orientation. Given a model of leaf normal orientation, one can estimate the gap fraction as $\exp(-G(0)\mathrm{LAI})$. Thus, the fraction of PAR absorbed by the ground together with independent estimates of LAI can potentially be used to derive at least three measures of canopy structure — (1) extinction coefficient, $G/\cos(\theta_0)$, for use in ecological models, which typically use the Beer's law or two-stream approximation to model radiation, (2) derive estimates of mean leaf inclination and (3) the gap fraction along the near-nadir direction which is related to vegetation ground cover.

It should be noted that the BHRPAR and FPAR are derived from two independent algorithms using different input information. The broadband visible albedo is directly obtained from the spectral BHR by integrating this product over the photosynthetically active spectral region (Diner et al., 1999a,b). In the MISR approach to FPAR retrieval, BHR and BRF in the red and NIR spectral bands are used to estimate LAI and canopy absorptance at the red spectral wavelength. The latter then is extrapolated from one spectral point to the entire PAR region

Table 1
Validation sites, availability of MISR BHR and reference LAI maps

Site	Lat/Lon	Biome type	Availability of red band MISR BHR for 2° by 2° area	Date of field campaign	Sampling area	Field LAI		Reference LAI map		Reference
						Mean	STD	Area	Mean LAI	
Konza	39.08N/ 96.56W	Grasses	23%	June, 2000 August, 2000 July, 2001	100 25×25 m Plots	1.96 2.02 2.9	0.62 0.81 0.85	7×7 km	2.0∼2.9	Cohen et al. (2003)
Bondville	40.01N/ 88.29W	Broadleaf crops	20%	July, 2000 August, 2000		2.47 3.6	1.5 0.87	7×7 km	2.5∼3.6	
Harvard Forest	42.54N/ 72.17W	Broadleaf forests	15%	June, 2000 August, 2000 July, 2001		5.08 4.99 5.54	0.85 0.67 0.81	7×7 km	4.3 4.9	
Mongu	15.43S/ 23.25E	Savannas	40%	April 20,2000 September 02, 2000	750×750 m Transect	1.9 0.8	1 0.5	n/a	n/a	Privette et al., 2002; Huemmrich et al., 2005
Alpilles	43.81N/ 4.75E	Cropland	30%	Feb 26–March 15, 2001	3×3 km	n/a	n/a	16×16 km	∼0.9	Tan et al. (2005)

using the canopy spectral invariant (Knyazikhin et al., 1998b; Panferov et al., 2001; Rautiainen & Stenberg, 2005; Smolander & Stenberg, 2003, 2005; Wang et al., 2003). Thus BHRPAR and FPAR can be treated as independent estimates of canopy reflective and absorptive properties. The analyses presented here, therefore, suggest the consistency and complementarity of the MISR surface product suite that includes LAI, FPAR and BHRPAR.

4. MISR land surface products over validation sites

The EOS land community provides the infrastructure to accumulate resources required for validation of satellite products by linking multiple field programs (Morisette et al., 2006). At most of the sites included in this structure, there is a long-term measurement program to support in situ measurements that can be used to assess the quality of satellite products. We selected five validation sites to analyze the MISR Level 2 Surface Parameters Product at local scales. The selected sites are shown in Table 1. MISR data from year 2000 were selected for this investigation as in situ LAI measurements were available from most of these sites for this period.

4.1. Availability of MISR surface reflectance data

A successful retrieval of the BHR in the red band is necessary to perform LAI/FPAR retrievals. Therefore, we examine the availability of red band BHR product at local scales by evaluating the ratio of pixels with valid (non-fill) BHR values to the total number of pixels. The analysis was performed for 2° by 2° areas centered on the validation sites. For each area, the ratio was calculated using pixels from all Year 2000 orbits that overlapped with the 2° by 2° area. The availability of MISR BHR changes with site and varies between 15% and 40% (Table 1). On average, input valid for LAI/FPAR retrievals was successfully generated for about 25% of the pixels. A significant portion of pixels with invalid input appeared to be cloud contaminated as the following analysis will demonstrate.

Inputs to the MISR surface retrieval algorithm include several atmospheric parameters from the MISR Aerosol Product. A successful retrieval must be done as a prerequisite to performing any type of surface retrieval (Martonchik et al., 1998a, 2002). A "Stage 1" aerosol retrieval algorithm (Diner et al., 2001) generates a Retrieval Applicability Mask (RAM) which contains flags indicating either a pixel is acceptable for the aerosol retrieval process or the name of the test which resulted in an unusable or contaminated designation. If data are not available in all 36 (angular and spectral) channels of MISR, the tests are skipped and the flag is set to 253. A complete list of flag values is presented in Table 2. Their precise definitions can be found in Diner et al., 2001.

A statistical summary of the RAM flags for two sites that exhibit minimum data availability is shown in Fig. 7. The failure results are mainly generated by the angle-to-angle correlation test (45%–50%). The failure of the angle-to-angle smoothness test is the second factor (about 9%) preventing the aerosol retrieval process. Results from the remaining tests average between 8% and 17%. The percentage of pixels with flag value "253" varies between 14% and 22%. Distributions of the RAM

Table 2
MISR retrieval applicability mask

Flag	Flag description/test name
0	Clear
1	Missing data test
2	Poor quality test
3	Glitter contamination test
4	Topography obscuration test
5	Topography shadow test
6	Topographic complexity evaluation test
7	Not used
8	Cloud shadow test (not implemented)
9	Angle-to-angle smoothness test
10	Angle-to-angle correlation test
11	Region not suitable
12	Optically thick atmosphere
253	Fill value

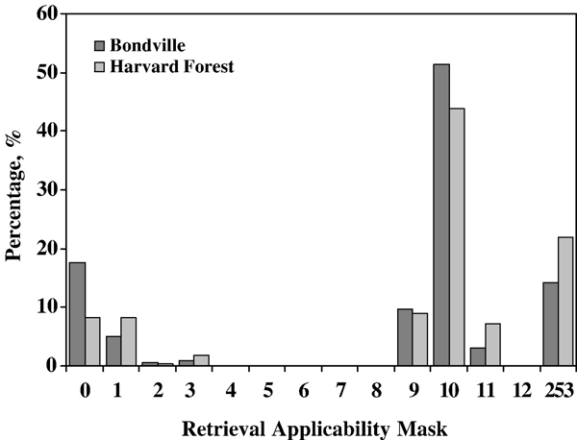

Fig. 7. Statistical summary of the RAM flags for Bondville and Harvard Forest sites.

flags for other sites exhibit similar behavior (Hu et al., 2004). These results can be interpreted as follows.

The imagery is put through a cloud-screening process before any aerosol retrievals are performed using MISR data (Martonchik et al., 2002). A number of tests (Table 2) are performed to identify all areas in a scene that are considered not suitable for aerosol retrieval due to clouds or other reasons. Note that the radiance angle-to-angle smoothness (#9) and the image angle-to-angle correlation (#10) tests are performed using multi-angle imagery that has been radiometrically calibrated, coregistered, and geolocated to the terrain. As such, if there are any clouds occurring within a scene, they will appear to be misregistered because of parallax. Since these two tests are designed to detect any such misregistrations, they provide a measure of cloud screening. Currently, these tests frequently override a flag value "optically thick atmosphere" (#12) generated by a cloud decision matrix.

To summarize, (1) cloud contamination is the main reason why a limited number of valid data are available for LAI/FPAR retrievals. In about 50%–60% of the cases examined, failure of the radiance angle-to-angle smoothness (# 9) and the image angle-to-angle correlation (#10) tests prevented aerosol retrieval. (2) The absence of data in all 36 channels of MISR (flag value "253") is responsible for about 14%–22% of invalid input to the LAI and FPAR algorithm. (3) The failure rate of other tests (Table 2) for the selected areas is about 8%–17%. (4) When a successful aerosol retrieval is performed, there is a 95% probability of successful surface reflectance retrieval (Martonchik, personal communication).

4.2. LAI and FPAR retrievals

The availability of LAI and FPAR products was performed for the same 2° by 2° areas centered on the validation sites. For each area, pixels from all orbits in year 2000 that overlapped with the 2° by 2° area were separated into three categories where (i) LAI/FPAR retrievals were not performed due to unavailability of BHR in the red and NIR spectral bands; (ii) LAI/FPAR algorithm failed and (iii) successful LAI/FPAR retrievals were performed. The first category, in turn, was broken into unavailability of input "due to clouds" and "due to other reasons." Fig. 8 shows a statistical summary of these cases. On average, about 25% of the pixels contain valid input to the LAI/FPAR algorithm. This number changes by site and may be as low as 14%.

The LAI/FPAR algorithm performance can be further assessed by analyzing the seasonal course of the Retrieval Index (RI) defined as the ratio of the number of pixels with successful LAI/FPAR retrievals to the total number of pixels with valid input. This index does not indicate retrieval quality but rather the success rate of the algorithm. Fig. 9 shows temporal variation in the RI for 2° by 2° areas centered on the five sites described in Table 1 and a needle leaf forest site near Ruokolahti, Finland (61.32N/28.43E, Wang et al., 2004). The low number of algorithm retrievals during the winter time is due to snow conditions and/or the absence of green leaves. The retrieval index varies between 50% and 80% during the summer time.

Fig. 10 shows temporal variation in mean LAI values over 2° by 2° areas. Such a large area was required to accumulate sufficient statistics needed to derive mean temporal trajectories in view of the poor spatial coverage of the product. To reduce the impact of biome heterogeneity, mean LAI at a given validation site was derived from pixels with the correct biome type. Visual inspection of Fig. 10 indicates a significant overestimation of LAI in cases of biomes 1 (grasses and cereal crops) and 3 (broadleaf crops). The problem was traced to the calibration of the algorithm. The calibration procedure was performed by deriving global biome-dependent patterns of surface reflectance first and then adjusting a number of configurable parameters in the algorithm to match observations and simulations (Hu et al., 2003; Tian et al., 2003). The at-launch land cover map based on AVHHR data was used to select biome

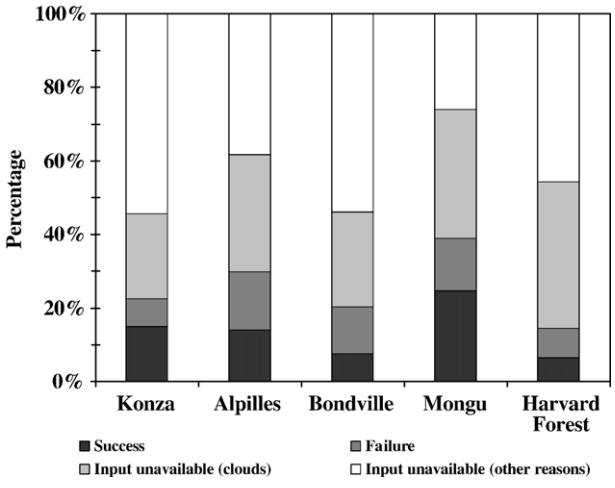

Fig. 8. Statistical summary of cases for which (i) a successful LAI/FPAR retrieval was performed; (ii) LAI/FPAR algorithm failed; and (iii) a LAI/FPAR retrieval was not performed due to the absence of input. The latter case is broken into two sub-categories: "Input is unavailable due to clouds" and "Input is unavailable due to other reasons." The statistical analysis is performed using all Year 2000 orbits that overlapped with the 2° by 2° areas centered on the selected validation sites.

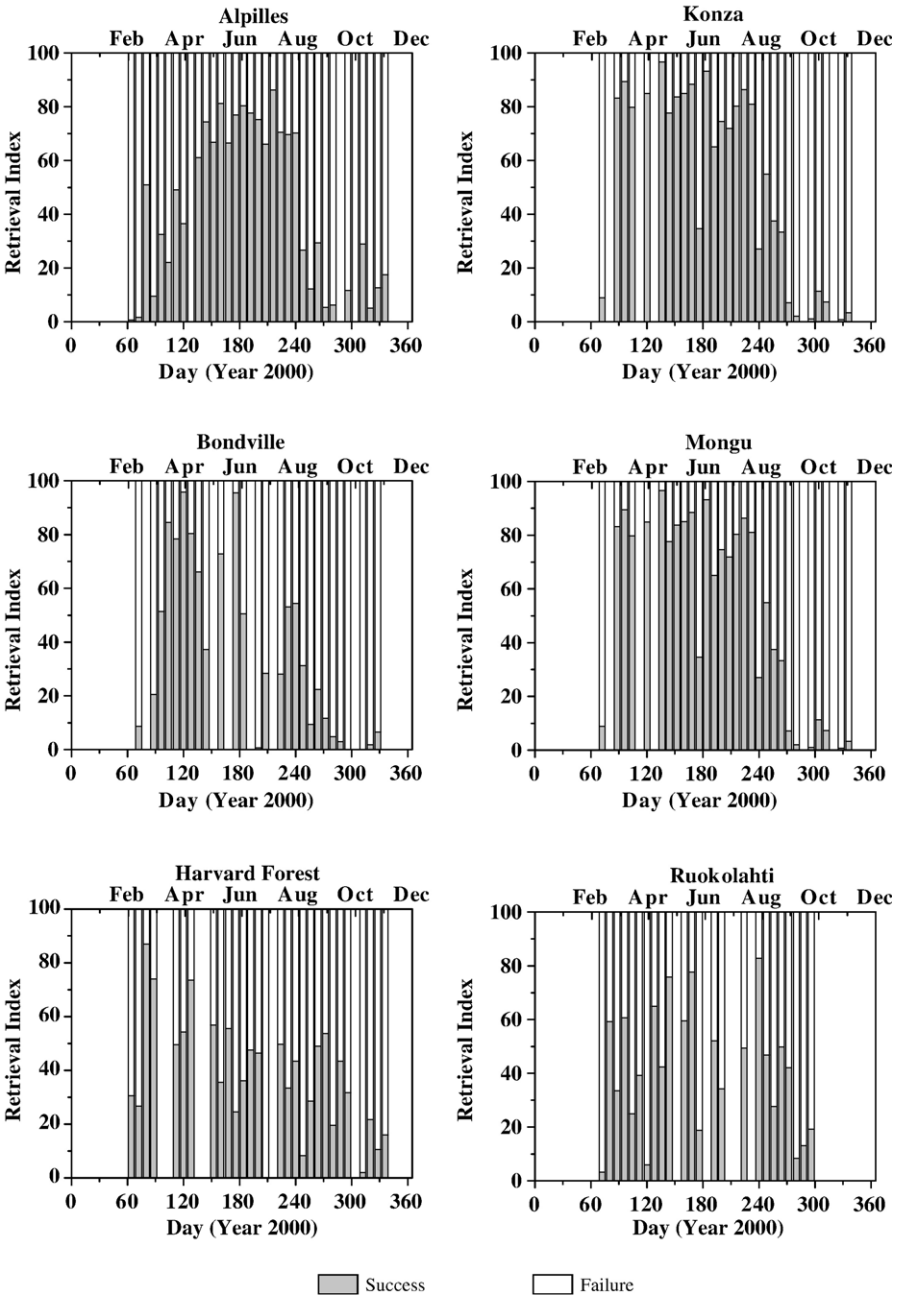

Fig. 9. Temporal variation in the retrieval index for six validation sites.

dependent surface reflectances. It was found (Yang et al., 2006) that this land cover map has significant misclassification between grasses (biome 1) and broadleaf crops (biome 3), resulting in the mismatch between simulated and actual observations of the surface reflectance. The algorithm was recalibrated with Collection 3 MODIS Land Cover Product and integrated into version 3.3 MISR LAI/FPAR software which become operational since May 2005. Fig. 11 shows temporal profiles of mean LAI generated by the recalibrated algorithm.

The LAI trajectories show expected seasonal variations with the exception of needleleaf forests. The strong LAI seasonality in needleleaf forests is spurious and must be treated as an artifact resulting from too few reliable winter time retrievals (Fig. 8). It should also be noted that there are few reliable measurements in the high northern latitudes during the winter period because of low sun angles and weak illumination conditions, which further amplify the problem of reliably estimating LAI in these regions during the winter months.

5. Validation of MISR LAI product

Validation results are a key source of information to users on product accuracy and also serve as the basis for further algorithm and product refinement research. Product validation

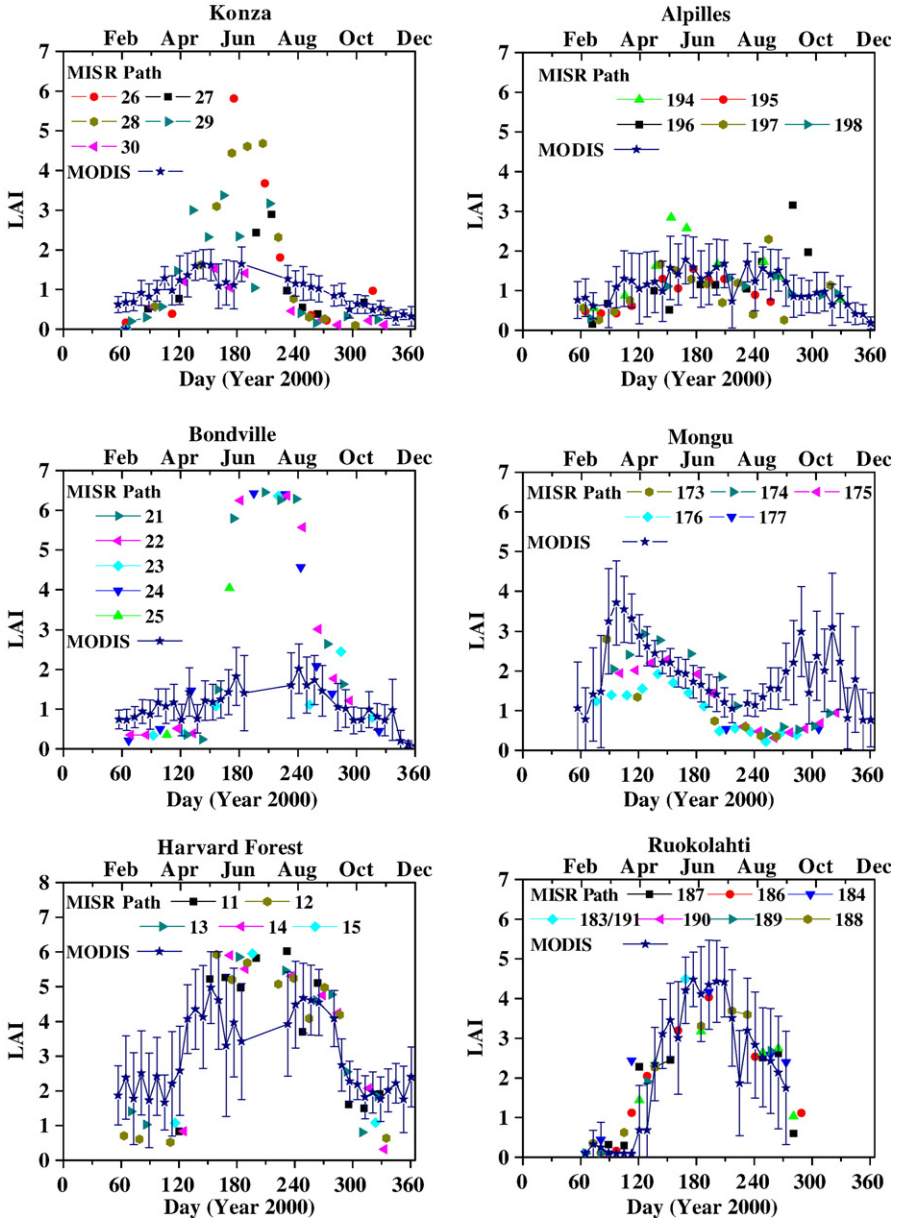

Fig. 10. Annual profiles of the mean LAI temporal variation derived from MODIS (line) and MISR (symbols) data for Konza, Alpilles, Bondville, Mongu, Harvard Forest and Ruokolahti sites. Symbols in the MISR LAI profile corresponds mean values over different paths overlapped with 2° by 2° areas centered on the validation site.

refers to assessment of product accuracy through comparisons to ground measurements that are scaled to the product resolution (Morisette et al., 2002). Significant efforts have already been made by multiple international teams to validate the Terra MODIS LAI product (Yang et al., 2006). Part of validation activities were carried out at validation sites used in this study (Table 1). For most of the sites, the validation procedure includes generation of a fine LAI resolution map, typically 7 by 7 km, from ground measurements and high-resolution satellite imagery according to a specific algorithm. This map is then degraded to a moderate resolution which is used as a reference to assess the quality of satellite products. We detail this validation strategy for Alpilles site in France.

5.1. Validation of the LAI product at a cropland site in Alpilles

A field campaign over a 3×3 km^2 agricultural area near Alpilles in France (43.810°N, 4.750°E) was performed from February 26 to March 15 in year 2001 (Baret et al., 2006). More than 95% of this site was composed of young and mature wheat and grasses (biome 1). Leaf area index was measured with a LAI-2000 Plant Canopy Analyzer. Data were collected on two transects of about 1 km at 50 m intervals and at 15 locations scattered throughout the site. Measurements at the 15 locations were performed at 4 m intervals on two 20 m lines which formed a regularly shaped cross. The average of 12 measurements was assigned as the LAI value at each of these locations

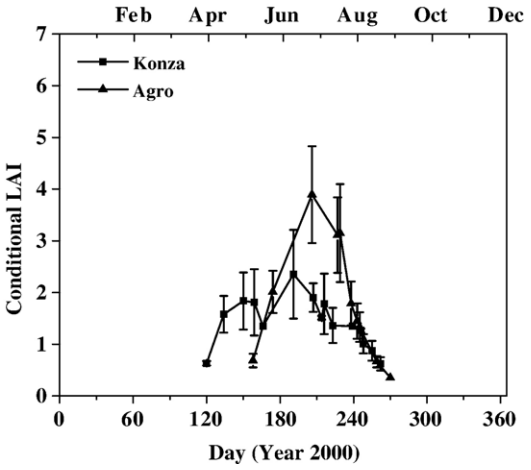

Fig. 11. Annual profiles of the mean LAI temporal variation over biome 1 (grasses and cereal crops) and biome 3 (broadleaf crops) in 0.5° by 0.5° areas centered on Konza and Bondville sites generated by the re-calibrated (version 3.3) LAI and FPAR algorithm.

and the standard deviations were taken as the precision of field measured LAI.

A subset of an ETM+ image from March 15, 2001 (path 196, row 90) containing the Alpilles site was selected for the purpose of generating a fine resolution LAI map of the site. The image was atmospherically corrected using the 6S radiative transfer code (Vermote et al., 1997). Various techniques, including an empirical regression based on the Simple Ratio and the fine resolution MODIS LAI/FPAR algorithm, were evaluated to identify the most accurate method for generating the fine resolution LAI maps. The fine resolution MODIS algorithm and the SR relationship were the best candidates for this site and thus were used to generate a 30 m LAI map of a 20 × 20 km area centered on the Alpilles site (Tan et al., 2005). This map was re-projected from UTM WGS84 projection into the Space Oblique Mercator (SOM) projection using the ENVI (version 4) software (WWW4) first and then degraded to a 1.1 km resolution reference map (Fig. 12). Biome 1 pixels were selected for further analysis.

The MISR data from path 196, orbit 6598 (March 15, 2001) were used to validate the version 3.3 MISR LAI product. A 16.5 × 16.5 km area (15 × 15 MISR pixels) which coincided with the reference map was extracted from this path. There were 125 biome 1 pixels in the reference map. The MISR LAI/FPAR algorithm successfully retrieved LAI values for 65 of these pixels. Fig. 13 shows distributions of the version 3.3 MISR LAI product and the reference LAI. Mean LAIs derived from the MISR and reference maps are 0.84 (std = 0.3) and 0.96 (std = 0.29), respectively. This result suggests that the MISR LAI product for this site is accurate to within an accuracy of about 0.2 LAI with a precision of 0.3. This statement refers to an area consisting of about 65 MISR pixels (about 9 × 9 km).

5.2. Validation of MISR LAI product at other sites

An analysis of the availability of MISR observations over the remaining sites showed that 0.5° by 0.5° or larger areas around the sites were required to accumulate statistically stable LAI retrievals needed for the analysis described earlier. The reference maps of such sizes (see Table 1) were not available. The Collection 4 MODIS LAI product was taken as the reference. Validation at stage 1 has been achieved for the MODIS LAI and FPAR product. Field measurements from 29 sites, representative of major global vegetation types, were regressed against corresponding MODIS LAI pixel values, with a resulting R^2 value of 0.87 and an RMSE of 0.66. The MODIS LAI overestimates field measurements by about 12% in dense vegetation (Yang et al., 2006). The assessment of the MISR product will be accomplished via analyses of linear regression models $Y = \beta X + \alpha$ of MISR LAI (dependent variable Y) with respect to the MODIS LAI (independent variable X).

Several complicated issues arise when one attempts to implement this strategy. For example, the actual spatial location of the corresponding pixels in the two product maps may not match well because of geolocation uncertainties as well as

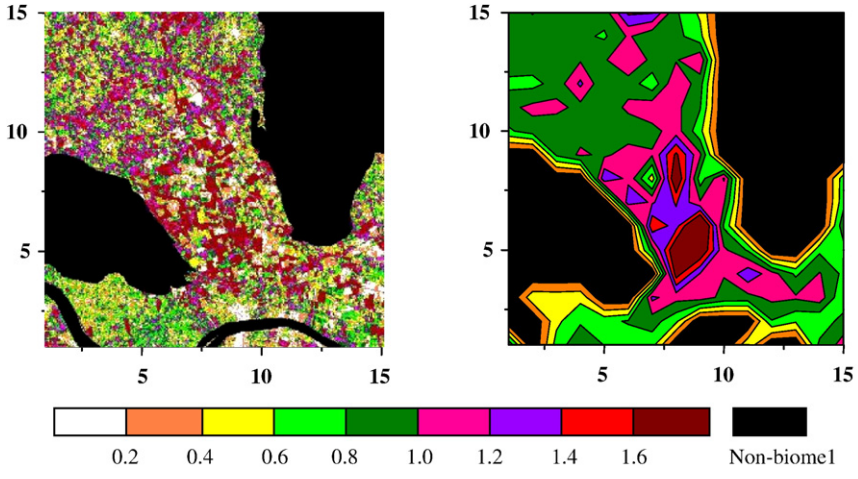

Fig. 12. Reference LAI maps at 30 m (left panel) and 1.1 km (right panel) resolutions over 16.5 km × 16.5 km (15 × 15 MISR pixels) area in Alpilles. The maps are projected on the MISR Path 196 Space Oblique Mercator (SOM) projection.

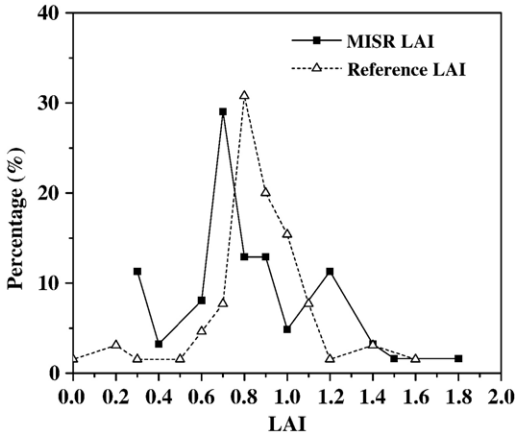

Fig. 13. Distribution of the version 3.3 MISR LAI and reference LAI values at a resolution of 1.1 km for the Alpilles site.

reprojection and resampling procedures. Also, satellite derived products themselves have a certain accuracy and precision, for example, due to incomplete atmospheric correction. Therefore, the LAI value assigned to a single pixel may be unreliable, but the mean LAI of multiple pixels may be valid (Wang et al., 2004). Thus, it is preferable to perform comparisons at multi-pixel (patch) scale, where the LAI product is statistically stable.

Analyses of MISR and MODIS LAI were performed for 0.5° by 0.5° areas centered on the validation sites. For each 8-day MODIS composite period, mean MODIS and MISR LAI values were accumulated over MISR paths that overlay the 0.5° by 0.5° area and whose orbits fall within the MODIS compositing period. These mean values were then used to build linear regression models of MISR LAI with respect to the MODIS LAI. The relationships between the MISR conditional LAI and MODIS LAI values for four biome types are shown in Fig. 14.

The BigFoot team (WWW5) performed validation of MODIS LAI products at Bondville, a cropland site in Illinois, USA; Konza Prairie Biological Station, Manhattan, Kansas, USA; and the Harvard Forest, (a temperate mixed forest site in Massachusetts, USA) sites (Cohen et al., 2003). At Konza and Bondville, Collection 4 MODIS LAI was close to BigFoot field measurements scaled to MODIS resolution. MODIS and MISR LAI products agree sufficiently well at the Konza site (Fig. 14). Together with the Alpilles results described earlier, this suggests good agreement between MISR LAI retrievals and ground measurements. The correlation between MISR and MODIS LAIs is stronger at the Bondville site (R^2=0.88), the slope is 1 and the offset is −0.4. The MISR product underestimates MODIS LAI by about 0.4 LAI which is within the product accuracy specification of 0.5 LAI. The MISR product underestimates MODIS LAI by 0.9 LAI at the Harvard Forest site. This result may indicate better MISR retrievals since MODIS overestimates ground measurements (Cohen et al., 2003).

The spatial and temporal variation of the MODIS LAI product in southern Africa was validated by Privette et al. (2002)

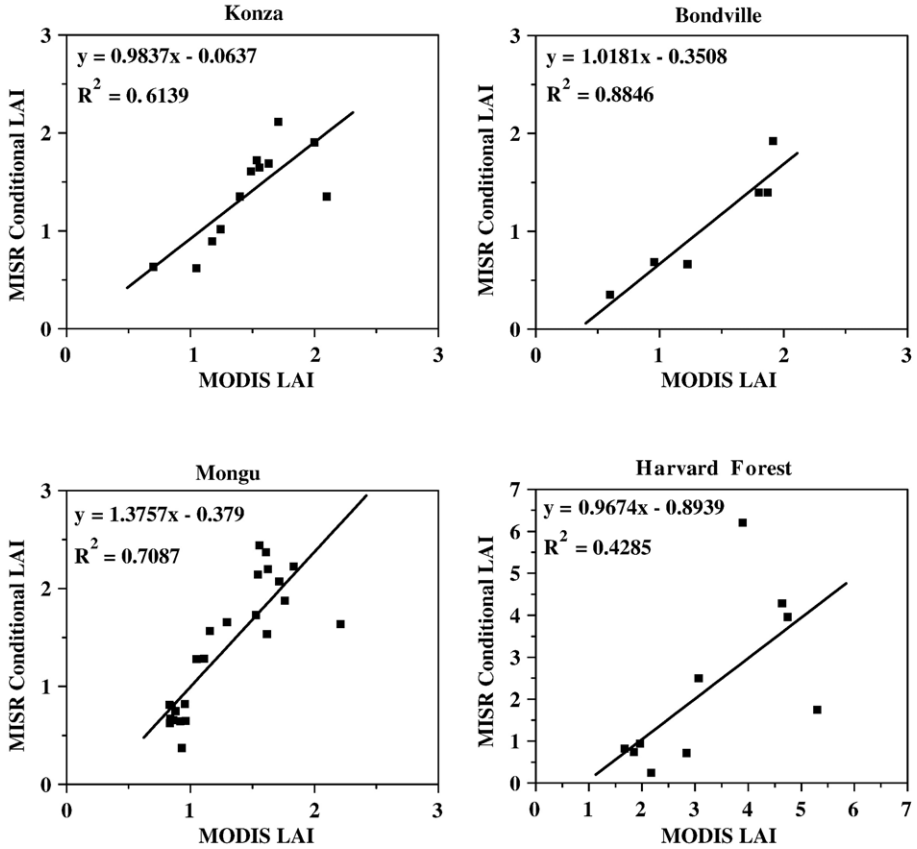

Fig. 14. Linear regression models of MISR LAI with respect to the MODIS LAI for 4 validation sites. Symbols represent multi-temporal patches.

and Huemmrich et al. (2005) along the International Geosphere Biosphere Programme's (IGBP) Kalahari Transect. Mongu in Zambia was one of five sites incorporated in this large-scale transect. At this site, field data were collected from March through December 2000. The TRAC instrument was used to sample the vegetation overstory LAI along three 750-m transects separated by 250 m. The length and spacing of transects were chosen to sample an area large enough to be representative of a 1-km MODIS pixel. The direct outcome of TRAC, plant area index, was adjusted with ancillary stem area index data to estimate the LAI. The results indicate that the MODIS LAI product correctly captured the temporal phenology including the wet season peak (April), senescence (May through July), peak dry season (September) and green-up (November). The MISR product also captures this behavior (Fig. 10). MODIS and MISR LAIs are well correlated, $R^2=0.7$ (Fig. 14). However, the MODIS LAIs exhibit a smaller range of variation compared to MISR LAIs. This is because MODIS overestimates LAI values by about 0.4 LAI during the dry season (see Fig. 8 in Privette et al., 2002). This results in an increased value of the slope in the regression model ($\beta=1.4$). If one corrects overestimated values by 0.4, the slope and intercept become 1 and 0.1, respectively, suggesting that the MISR provides a more accurate estimate of LAI during the dry seasons and coincides with MODIS values during other periods. This is consistent with the example discussed in Section 3.2.

6. Conclusions

An algorithm for the retrieval of LAI and FPAR from MISR surface reflectance data has been in operational processing at the Langley ASDC since October 2002. This paper describes the research basis for transitioning the MISR LAI/FPAR product from provisional to "stage 1 validated" status, i.e., an estimation of product accuracy has been made using a small number of independent measurements from selected locations and time periods and ground-truth/field program effort. In our approach, a comprehensive analysis of relationships, consistency and complementarity between various MISR surface products derived from independent algorithms is also included to demonstrate the potential utility of these MISR products in monitoring and modeling studies as well as to explore the potential for enhanced information retrieval through innovative manipulation of multiple products. At the present time, most of the validation efforts are limited to LAI, and only a few FPAR measurements are available over select locations. Therefore, most of the material in this paper is focused on the LAI product.

The location of reflectance data in the spectral space is the basic source of information about the vegetation canopy conveyed by single angle multispectral satellite data. The inclusion of multiangular data (in addition to spectral sampling) provides additional information on land cover type, heterogeneity of vegetation canopies and brightness of their background. The use of this information results in reduced ambiguity and error in the retrieved LAI and FPAR fields in arid lands. The consistency and complimentarity of the parameters in the MISR surface product suite that includes LAI, FPAR and BHRPAR is demonstrated here in the derivation of the canopy extinction coefficient, mean leaf angle inclination and the gap fraction.

The spatial coverage of the MISR LAI/FPAR product is limited by the availability of atmospherically corrected surface reflectance data that are input to the algorithm. Cloud contamination is the principal reason limiting the availability of reflectance data. Failure of the radiance angle-to-angle smoothness and the image angle-to-angle correlation tests prevented aerosol retrieval in about 48–56% of the cases examined. The absence of data in all 36 channels of MISR is responsible for about 13–21% of invalid input to the LAI and FPAR algorithm. These pixels are mainly located near the path edges where the deviation of MISR view angles from their nominal values is maximal. The failure rate due to other reasons is about 7–17%.

Validation of the early versions of the MISR LAI product suggests the algorithm overestimates LAI values in grasses and broadleaf crops. The algorithm was recalibrated and incorporated into the version 3.3 operational MISR software. Validation of this version suggests the MISR LAI product to correctly accommodate structural and phenological variability. The product is accurate to within 0.66 LAI in herbaceous vegetation and savannas and is an overestimate by about 1 LAI in broadleaf forests. Retrievals over needle leaf forests remain at provisional quality level.

Acknowledgement

The research of J. Hu, Y. Su, Y. Knyazikhin and R. B. Myneni is performed at Boston University under contract with the Jet Propulsion Laboratory, California Institute of Technology as part of the EOS-MISR project.

Appendix A. WWW sites

WWW1: EOS Core Validation Sites, http://landval.gsfc.nasa.gov/MODIS/index.php

WWW2: NASA Langley Atmospheric Sciences Data Center, http://eosweb.larc.nasa.gov/

WWW3: Land Processes Distributed Active Archive Center, http://edcimswww.cr.usgs.gov/pub/imswelcome/

WWW4: ENVI software, http://www.rsinc.com/envi

WWW5: BigFoot project, http://www.fsl.orst.edu/larse/bigfoot/

References

Baret, F., Morisette, J., Fernandes, R. A., Champeaux, J. L., Myneni, R., Chen, J., et al. (2006). Evaluation of the representativeness of networks of sites for the global validation and intercomparison of land biophysical products: Proposition of the CEOS-BELMANIP. *IEEE Transactions on Geoscience and Remote Sensing*, *44*(7), 1794–1803.

Bronshtein, I. N., & Semendyayev, K. A. (1985). *Handbook of mathematics.* Berlin: Springer 973 pp.

Buermann, W., Dong, J., Zeng, X., Myneni, R. B., & Dickinson, R. E. (2001). Evaluation of the utility of satellite based vegetation leaf area index data for climate simulations. *Journal of Climate*, *14*(17), 3536–3550.

Cohen, W. B., Maiersperger, T. K., Yang, Z., Gower, S. T., Turner, D. P., Ritts, W. D., et al. (2003). Comparisons of land cover and LAI estimates derived

from ETM+ and MODIS for four sites in North America: A quality assessment of 2000/2001 provisional MODIS products. *Remote Sensing of Environment*, *88*, 233−255.

de Wit, C. T. (1965). *Photosynthesis of leaf canopies.Agric. Res. Report*, *Vol. 663*. Wageningen 57 pp.

Diner, D. J., Asner, G. P., Davies, R., Knyazikhin, Y., Muller, J. P., Nolin, A. W., et al. (1999). New directions in Earth observing: Scientific application of multi-angle remote sensing. *Bulletin of the American Meteorological Society*, *80*(11), 2209−2228.

Diner, D., Abdou, W. A., Ackerman, T. P., Crean, K., Gordon, H. R., Kahn, R. A., et al. (2001). *Level 2 aerosol retrieval algorithm theoretical basis.*: Jet Propulsion Laboratory, California Institute of Technology 24 pp.

Diner, D. J., Braswell, B. H., Davies, R., Gobron, N., Hu, J., Jin, Y., et al. (2005). The value of multiangle measurements for retrieving structurally and radiatively consistent properties of clouds, aerosols, and surfaces. *Remote Sensing of Environment*, *97*, 495−518.

Diner, D. J., Martonchik, J. V., Borel, C., Gerstl, S. A. W., Gordon, H. R., Myneni, R. B., et al. (1999). *Level 2 surface retrieval algorithm theoretical basis.* Jet Propulsion Laboratory, California Institute of Technology 93 pp.

Hu, J., Su, Y., Myneni, R. B., & Knyazikhin, Y. (2004, December). LAI/FPAR validation status and updates to CART. *Presentation at MISR Science Team meeting, Pasadena, CA*.

Hu, J., Tan, B., Shabanov, N., Crean, K. A., Martonchik, J. V., Diner, D. J., et al. (2003). Performance of the MISR LAI and FPAR algorithm: A case study in Africa. *Remote Sensing of Environment*, *88*, 324−340.

Huemmrich, K. F., Privette, J. L., Mukelabai, M., Myneni, R. B., & Knyazikhin, Y. (2005). Time-series validation of MODIS land biophysical products in a Kalahari Woodland, Africa. *International Journal of Remote Sensing*, *26* (19), 4381−4398.

Kaufmann, R. K., Zhou, L., Knyazikhin, Y., Shabanov, N. V., Myneni, R. B., & Tucker, C. J. (2000). Effect of orbital drift and sensor changes on the time series of AVHRR vegetation index data. *IEEE Transactions on Geoscience and Remote Sensing*, *38*(6), 2584−2597.

Kiehl, J. T., Hack, J. J., Bonan, G. B., Boville, B. A., Briegleb, B. P., Williamson, D. L., et al. (1996). *Description of the NCAR Community Climate Model (CCM3) Tech. Rep. NCAR/TN-420+STR.* Boulder, CO: National Center for Atmospheric Research 152 pp., Available from NCAR, P.O. Box 3000, Boulder, CO 80307.

Kiehl, J. T., Hack, J. J., Bonan, G. B., Boville, B. A., Williamson, D. L., & Rasch, P. J. (1998). The national center for atmospheric research community climate model: CCM3. *Journal of Climate*, *11*, 1131−1149.

Knyazikhin, Y., & Marshak, A. (2000). Mathematical aspects of BRDF modeling: Adjoint problem and Green's function. *Remote Sensing Reviews*, *18*, 263−280.

Knyazikhin, Y., Martonchik, J. V., Diner, D. J., Myneni, R. B., Verstraete, M., Pinty, B., et al. (1998). Estimation of vegetation canopy leaf area index and fraction of absorbed photosynthetically active radiation from atmosphere-corrected MISR data. *Journal of Geophysical Research*, *103*, 32239−32256.

Knyazikhin, Y., Martonchik, J. V., Myneni, R. B., Diner, D. J., & Running, S. W. (1998). Synergistic algorithm for estimating vegetation canopy leaf area index and fraction of absorbed photosynthetically active radiation from MODIS and MISR data. *Journal of Geophysical Research*, *103*, 32257−32274.

Martonchik, J. V., Diner, D. J., Crean, K. A., & Bull, M. A. (2002). Regional aerosol retrieval results from MISR. *IEEE Transactions on Geoscience and Remote Sensing*, *40*, 1520−1531.

Martonchik, J. V., Diner, D. J., Kahn, R. A., Ackerman, T. P., Verstraete, M. M., Pinty, B., et al. (1998). Techniques for the retrieval of aerosol properties over land and ocean using multi-angle imaging. *IEEE Transactions on Geoscience and Remote Sensing*, *36*, 1212−1227.

Martonchik, J. V., Diner, D. J., Pinty, B., Verstraete, M. M., Myneni, R. B., Knyazikhin, Y., et al. (1998). Determination of land and ocean reflective, radiative, and biophysical properties using multi-angle imaging. *IEEE Transactions on Geoscience and Remote Sensing*, *36*, 1266−1281.

Morisette, J. T., Baret, F., Privette, J. L., Myneni, R. B., Nickeson, J., Garrigues, S., et al. (2006). Validation of global moderate resolution LAI Products: A framework proposed within the CEOS Land Product Validation subgroup. *IEEE Transactions on Geoscience and Remote Sensing*, *44*(7), 1804−1817.

Morisette, J. T., Privette, J. L., & Justice, C. O. (2002). A framework for the validation of MODIS land products. *Remote Sensing of Environment*, *83*, 77−96.

Myneni, R. B., Nemani, R. R., & Running, S. W. (1997). Estimation of global leaf area index and absorbed par using radiative transfer models. *IEEE Transactions on Geoscience and Remote Sensing*, *35*, 1380−1393.

Panferov, O., Knyazikhin, Y., Myneni, R. B., Szarzynski, J., Engwald, S., Schnitzler, K. G., et al. (2001). The role of canopy structure in the spectral variation of transmission and absorption of solar radiation in vegetation canopies. *IEEE Transactions on Geoscience and Remote Sensing*, *39*(2), 241−253.

Privette, J. L., Myneni, R. B., Knyazikhin, Y., Mukelabai, M., Roberts, G., Tian, Y., et al. (2002). Early spatial and temporal validation of MODIS LAI product in the southern Africa Kalahari. *Remote Sensing of Environment*, *83*, 232−243.

Rautiainen, M., & Stenberg, P. (2005). Application of photon recollision probability in coniferous canopy reflectance model. *Remote Sensing of Environment*, *96*, 98−107.

Ross, J. (1981). *The radiation regime and architecture of plant stands.* Norwell, Mass: Dr. W. Junk 391 pp.

Sellers, P. J., Dickinson, R. E., Randall, D. A., Betts, A. K., Hall, F. G., Berry, J. A., et al. (1997). Modeling the exchanges of energy, water, and carbon between continents and the atmosphere. *Science*, *275*, 502−509.

Shabanov, N. V., Zhou, L., Knyazikhin, Y., Tucker, C. J., & Myneni, R. B. (2002). Analysis of interannual changes in northern vegetation activity observed in AVHRR data during 1981 to 1994. *IEEE Transactions on Geoscience and Remote Sensing*, *40*, 115−130.

Smolander, S., & Stenberg, P. (2003). A method to account for shoot scale clumping in coniferous canopy reflectance models. *Remote Sensing of Environment*, *88*, 363−373.

Smolander, S., & Stenberg, P. (2005). Simple parameterizations of the radiation budget of uniform broadleaved and coniferous canopies. *Remote Sensing of Environment*, *94*, 355−363.

Tan, B., Hu, J., Zhang, P., Huang, Shabanov, N., Weiss, M., et al. (2005). Validation of MODIS LAI product in croplands of Alpilles, France. *Journal of Geophysical Research*, *110*(D01107). doi:10.1029/2004JD004860

Tian, Y., Wang, Y., Zhang, Y., Knyazikhin, Y., Bogaert, J., & Myneni, R. B. (2003). Radiative transfer based scaling of LAI/FPAR retrievals from reflectance data of different resolutions. *Remote Sensing of Environment*, *84* (1), 143−159.

Vermote, E. F., Tanre, D., Deuze, J. L., Herman, M., & Morcrette, J. J. (1997). Second simulation of the satellite signal in the solar spectrum, 6S: An overview. *IEEE Transactions on Geoscience and Remote Sensing*, *35*, 675−685.

Wang, Y., Buermann, W., Stenberg, P., Voipio, P., Smolander, H., Häme, T., et al. (2003). A new parameterization of canopy spectral response to incident solar radiation: Case study with hyperspectral data from pine dominant forest. *Remote Sensing of Environment*, *85*, 304−315.

Wang, Y., Tian, Y., Zhang, Y., El-Saleous, N., Knyazikhin, Y., Vermote, E., et al. (2001). Investigation of product accuracy as a function of input and model uncertainties: Case study with seawifs and MODIS LAI/FPAR algorithm. *Remote Sensing of Environment*, *78*, 299−313.

Wang, Y., Woodcock, C. E., Buermann, W., Stenberg, P., Voipio, P., Smolander, H., et al. (2004). Evaluation of the MODIS LAI algorithm at a coniferous forest site in Finland. *Remote Sensing of Environment*, *91*, 114−127.

Yang, W., Tan, B., Huang, D., Rautiainen, M., Shabanov, N. V., Wang, Y., et al. (2006). MODIS leaf area index product: From validation to algorithm improvement. *IEEE Transactions on Geoscience and Remote Sensing*, *44* (7), 1885−1898.

Zhang, Y., Shabanov, N., Knyazikhin, Y., & Myneni, R. B. (2002). Assessing the information content of multi-angle satellite data for mapping biomes. II. Theory. *Remote Sensing of Environment*, *80*, 435−446.

Zhang, Y., Tian, Y., Knyazikhin, Y., Martonchick, J. V., Diner, D. J., Leroy, M., et al. (2000). Prototyping of MISR LAI and FPAR algorithm with POLDER data over Africa. *IEEE Transactions on Geoscience and Remote Sensing*, *38* (5), 2402−2418.

Zhang, Y., Tian, Y., Myneni, R. B., Knyazikhin, Y., & Woodcock, C. E. (2002). Assessing the information content of multi-angle satellite data for mapping biomes. I. Statistical analysis. *Remote Sensing of Environment*, *80*, 418−434.